Distribution Agreement

In presenting this thesis as a partial fulfillment of the requirements for a degree from Emory University, I hereby grant to Emory University and its agents the non-exclusive license to archive, make accessible, and display my thesis in whole or in part in all forms of media, now or hereafter now, including display on the World Wide Web. I understand that I may select some access restrictions as part of the online submission of this thesis. I retain all ownership rights to the copyright of the thesis. I also retain the right to use in future works (such as articles or books) all or part of this thesis.

Diego Jose Gonzalez Hernandez April 5, 2021

Modeling MWC 297's Complex Circumstellar Structure with Magnetically Supported Outflows

By

Diego Jose Gonzalez Hernandez

Alissa Bans, Ph.D.
Advisor

Department of Physics

Alissa Bans, Ph.D.
Advisor

Merida Batiste, Ph.D.
Committee Member

James Nagy, Ph.D.
Committee Member

2021

Modeling MWC 297's Complex Circumstellar Structure with Magnetically Supported Outflows

By

Diego Jose Gonzalez Hernandez

Alissa Bans, Ph.D.
Advisor

An abstract of
a thesis submitted to the Faculty of Emory College of Arts and Sciences
of Emory University in partial fulfillment
of the requirements of the degree of
Bachelor of Science with Honors

Department of Physics

2021

Abstract

Modeling MWC 297's Complex Circumstellar Structure with Magnetically Supported Outflows
By Diego Jose Gonzalez Hernandez

Motivated by the different properties of Herbig Be and Herbig Ae stars, we adapt a Monte Carlo Radiative Transfer code that has been successfully used to explain the observational data from Herbig Ae stars, in order to model magneto-rotationally driven dusty outflows around these objects. The adaptations we make generalize this approach to examine the Spectral Energy Distribution (SED) of MWC 297, a higher luminosity Herbig Be star. Furthermore, we developed an algorithm to produce Near Infra-Red (NIR) images of the target at a variety of different inclinations, which allows us to compare the simulations to existing NIR images of MWC 297 whose inclination is poorly constrained. We find that while dusty magnetically driven outflows alone can produce the observed NIR excess, high mass outflow rates are needed, a condition that worsens at higher inclinations. Consequently, we also examine the effects of several physically and observationally motivated modifications to the model. Namely, we consider the presence of an optically thick inner accretion disk (supported by multiple previous studies of MWC 297 and other Herbig Be sources), and setting the sublimation radius closer to the star. Though neither of these models with non-stellar emissions within the sublimation radius are fully consistently implemented, our data shows that both of their effects complement that of the dusty wind, and together they may play important roles in shaping the NIR emission of higher luminosity stars. Furthermore, their inclusion makes the inferred mass outflow rates more consistent with the literature. More work is needed to better model all these components consistently.

Modeling MWC 297's Complex Circumstellar Structure with Magnetically Supported Outflows

By

Diego Jose Gonzalez Hernandez

Alissa Bans, Ph.D.
Advisor

A thesis submitted to the Faculty of Emory College of Arts and Sciences
of Emory University in partial fulfillment
of the requirements of the degree of
Bachelor of Science with Honors

Department of Physics

2021

Acknowledgments

I would like to first acknowledge my advisor Dr. Alissa Bans for her endless support and help. Thank you for letting me work in multiple research projects throughout the past couple of years. These experiences, alongside with your lectures, have completely shaped my education and interests, and your guidance has allowed me to find my own path in the field that I am most passionate about.

I would also like to also extend my gratitude towards Dr. Merida Batiste. Thank you for your endless support and kindness. I have also thoroughly enjoyed the few projects that I have worked under your guidance, as well as all of your astronomy labs. Your guidance and enthusiasm always remind me of how exciting it is to study the cosmos.

I would also like to thank Dr. James Nagy. My studies in astronomy and physics have demonstrated how important numerical methods are to the field that I work in, and your Numerical Analysis class truly opened my eyes to the importance of understanding the machinery behind these approaches. It also showed me an academic area that I have increasingly become interested in, and that I intend to learn more from in the future.

Of course, I would also like to thank my family. I have an infinite gratitude towards my parents, whom have always been extremely supportive of my decisions. Their undying love and guidance have made me the person that I am today, and their encouragement never fails to remind me that, no matter how big the obstacles are, I can always keep pushing forward. Thanks also to my brother, with whom I have shared most of my life and with whom I have the most interesting conversations about any topic. Lastly, I would also like to thank the Guatemalan Association of Astronomy, for being one of the very few outreach groups in my country of origin. Your events were instrumental in creating my initial interest for astronomy when I was a child.

Finally, I want to again say thanks to my honors committee for all your feedback and accommodations. I appreciate the time each of you spent in your evaluation of my work and I am thankful for your input and your advice for me moving forward.

Contents

List of Figures

List of Tables

Chapter 1

Introduction

Stellar and planet formation are among the most fascinating research areas in astronomy. Over the past few decades, a lot of progress has been made in understanding the formation of lower mass stars ($\approx 1\ M_{\odot}$), through improved observational techniques and theoretical modeling of T-Tauri stars [4]. Progress in understanding the same processes for intermediate mass stars ($\approx 2 - 20\ M_{\odot}$) has been slower, however. These more massive counterparts of the T-Tauri stars are known as Herbig Ae/Be stars (HAeBe). HAeBe were first identified as being stars of spectral type A or B with emission lines that were associated with nebulostiy in its near proximity [5]. The definition was later refined after studying their Spectral Energy Distribution (SED), which demonstrated that these objects possess Near Infra-Red (NIR) and Infra-Red (IR) emissions that are above the expected by a stellar black body alone, and that could be explained by large amounts of circumstellar matter [6]. Further studies determined that HAeBe the NIR excess were explained by the presence of different types of circumstellar structures (such as disks [7] and outflows [8]). Consequently, a correct charac-

terization of the circumstellar structures around HAeBe stars presents a unique opportunity for understanding the formation of intermediate mass stars, as well as the environments in which planet formation could actively be taking place.

However, it is important to separate HAe and HBe stars, as they may posses significantly distinct environmental conditions near their vicinity. For instance, some studies have demonstrated how the strong NIR emission that HAe stars present may be well explained with magnetically driven outflows that posses an inner cavity [2]. On the other hand, HBe stars have generally been modeled with accretion disks [9]. Another major difference between these two types of stars is the amount of studies focusing in each. Since there has been a greater focus on HAe stars compared the HBe. Thus, further investigating the NIR excess present in HBe stars presents itself as an attractive opportunity, and an important point in the present study.

1.1 MWC 297

MWC 297 is one of the closest young massive stars, located at a distance of 375 pc. This makes it an exceptionally good object to study the physics behind star formation and early planet formation around high luminosity stars. Studies on MWC 297's optical spectrum have shown that it is a B1.5V star, and that it is highly attenuated due to reddening. Most of the estimates range from $A_v \approx 7.8$ to 8.3 mag [10] [11] [12]. In astronomical terms, this object is in the near vicinity to the Solar System. Consequently, it must be that the attenuation is mainly caused by the presence of a dense disk-like circumstellar structure made of dust which interacts with photons emitted by MWC 296. The existence of circumstellar dust is

Param.	Units	Value
distance	pc	375 ± 20
age	Myr	< 1
T_{eff}	K	23700
$log(L_{bol})$	$L_\odot$	4.59
M_*	$M_\odot$	16.9
R_*	$R_\odot$	4.59

Table 1.1: Best estimates for MWC 297's physical properties [3].

further supported by the excess of radiation in NIR observations, which gives MWC 297 the classification of a Herbig Be star [13] [14] [8]. MWC 297's physical properties are listed in table 1.1.

A large number of studies have been made regarding the geometry and nature of MWC 297's circumstellar structure. Observations in the milimiter range demonstrated that MWC 297's SED could be explained with a disk of radius of $\approx$ 43 AU [3]. However, a determination of the exact disk's structure in the vicinity of the star was still inconclusive. NIR interferometric observations mostly suggested that the radiation coming from MWC 297 was highly concentrated within a small region of 1.4 AU from the source [10]. In this scenario, geometric fits of the data indicated that MWC 297 possessed an almost face-on accreting disk [15]. On the other hand, more recent measurements obtained with the NRAO Very Large Array (VLA) and the IRAM Plateau de Bure (PdB) interferometers showed that a larger, non-accreting, and almost edge-on disk could also provide a satisfactory fit [3]. In this new model, the the 1.3 mm/2.7 mm spectral slope suggested the additional existence of a ring extending from 200 to 300 AU that is mainly composed of large grains of dust ($\approx$ 1 cm). Given that a larger number of studies supported the accretion disk model, the passive disk scenario went overlooked for a few years.

There is one major inconsistency, however. Spectroscopic measurements indicate that MWC 297 has a $v\ sin\ i = 350 \pm 50\ km\ s^{-1}$. This is in conflict with any moderately face-on model, as scenarios with inclinations between 15° and 40° could imply that MWC 297 has a rotational velocity $> 500\ km\ s^{-1}$, possibly above its critical velocity [10]. Indeed, recent calculations indicate that MWC 297's should have a breakup velocity of $\approx 480\ km\ s^{-1}$ [16] [17].

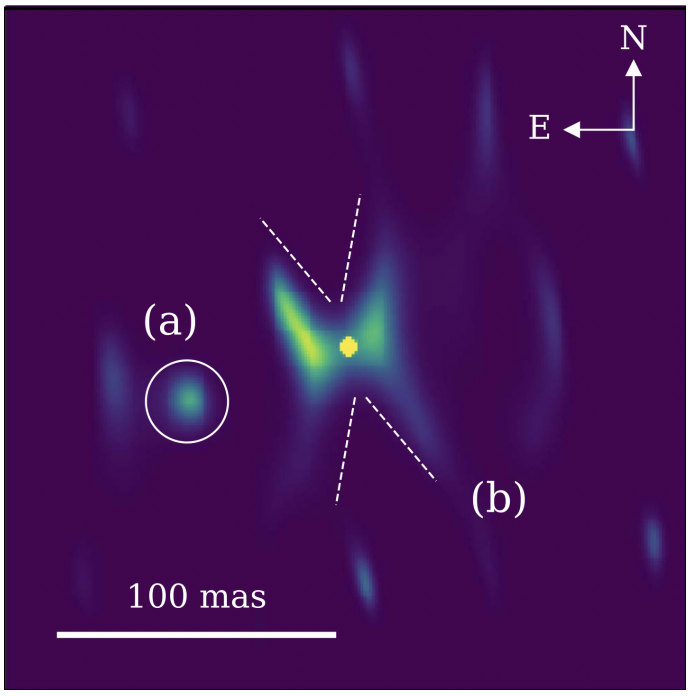

Figure 1.1: Reconstructed image of MWC 297 (a) is a companion candidate [1], and (b) is the outflow cavity.

Most recently, new 3.7 μm direct imaging of MWC 297 performed with the Large Binocular Telescope Interferometer has revealed an intricate circumstellar structure that completely forces to reconsider a variety of new models [1]. Figure 1.1 shows the reconstructed image from this observation. As it can be appreciated, a face-on accreting disk is not sufficient to explain MWC 297's morphology. The observed flux in this reconstruction shows a butterfly pattern that has also been observed in NIR HST images of protostars with outflows [18] [19]

[20]. Moreover, the observed brightness distribution is in agreement with disk with outflows observed at moderate inclinations ($> 50°$) [21], which eliminates the inconsistency of the $v\ sin\ i = 350 \pm 50\ km\ s^{-1}$.

Despite the large number of studies, it is evident that there are still questions surrounding MWC 297's structure and nature. Given the most recent results, in this study we explore the possibility of a magnetically supported and vertically distributed outflow as an explanation for MWC 297's NIR excess using a Monte Carlo Radiative Transfer (MCRT) scheme, with the intention to obtain a physically motivated model for MWC 297's circumstellar structure. The outline of the rest of this thesis is as follows: Chapter 2 explains the outflow models and parameters used in this study, Chapter 3 details the MCRT scheme and the methods used to analyze its outputs, and Chapter 4 presents the results and discussion.

Chapter 2

Outflow Models

2.1 Disk Winds

Centrifugally driven outflows can result from the transmission of torque from magnetic field lines crossing through a circumstellar disk to some of the charged particles residing in it. This transmission of magnetic torque affects the angular momentum of the particles involved, which in turn causes some of the disk's material to fall inward [22]. Consequently, the magnetic field lines are bent away from the disk's axis of rotation. The magnetic stress that this process provokes is capable of producing outflows in different directions [23]. However, it is common to assume that the material from the disk follows a path along the lines of the magnetic field [24]. It has been shown that the collisions between the gas in the wind and neutral particles in the disk can efficiently uplift dust above the disk's plane, creating a distribution of material that easily interacts with part of the central object's radiation. This process affects the photon's wavelengths, creating an excess in the NIR that can be observed [25].

Centrifugally driven winds caused by magnetic fields were originally used to model outflows in active galactic nuclei (AGN), as these objects also present certain excesses in the NIR [26]. However, the underlying physical principles governing the outflows in AGN are not too distinct to those underlying the outflows in young stellar objects (YSO). Particularly, it has been shown that the dusty disk-wind interpretation for the NIR excess can correctly model the SED from HAe stars [2], as centrifugally driven winds can efficiently uplift dust from the circumstellar disk. Figure 2.2 shows an illustration of this model. As we can appreciate, there are multiple parameters that we must adequately select to use the Disk-Wind model. Explaining our choices is the focus of the rest of this chapter.

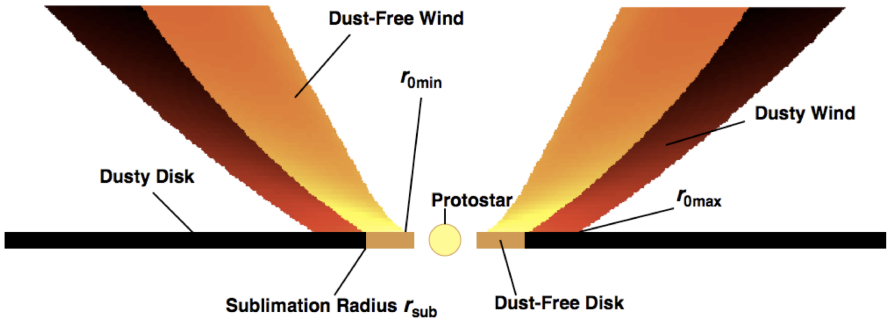

Figure 2.1: An illustration of a centrifugally driven disk wind in the vicinity of a protostar [2]. A detailed explanation of the parameters in this model can be found in Section 2.2.

2.2 Model Setup and Parameters

2.2.1 Gas density profile

To create a dusty wind model, we need to select a gas density profile. Semi-analytic solutions for the gas density structure can be calculated [23], and from these, analytical

approximations may be obtained [25]. We decide to use three representative wind solutions (named C, G and E), each one of them characterized by a different magnetic field line shape and density distribution [2]. Figure 2.2 presents a comparison of the magnetic field lines that define the outflow structure associated with each one of these three models. As we can appreciate, model C has the most vertical lines, and thus, a dusty wind of this type will directly intercept a larger portion of the stellar flux than the other two models. At the other end, model G has the most horizontal lines, and consequently intercepts the smallest proportion of the flux from the star. Finally, model E is in between the former two models. Additionally, Figure 2.3 shows a comparison of the density distributions related to these three models. It is clear that model C's density distribution decreases at a slower rate than the other two models, which further increases the number of interactions between the dusty wind and the star's flux.

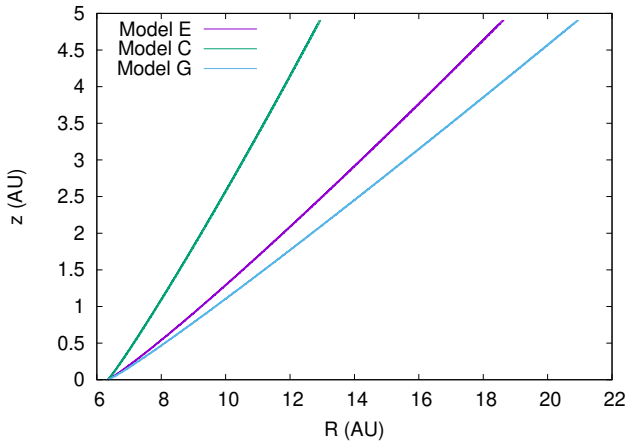

Figure 2.2: A comparison of the magnetic field lines in models E, C and G launched at the calculated R_{sub} for MWC 297 (see 2.2.3).

Another influential parameter of the dusty wind model is the outflow rate $\dot{M}$ at which the wind uplifts the disk's dust. Spectro-interferometric data taken with the Very Large Telescope Interferometer (VLTI) was used to fit models using the observed bracket gamma

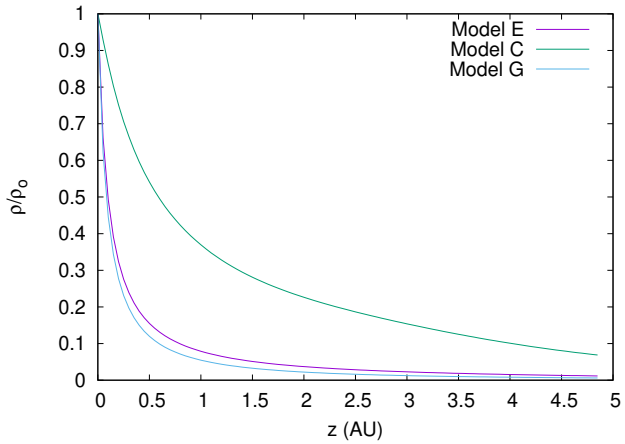

Figure 2.3: A comparison of the normalized density distribution used in models E, C and G. These density distributions are associated to the field lines shown in Figure 2.2.

emission (known to trace outflow and accretion rates). These models demonstrated that MWC 297 likely had a $\dot{M}$ with an order of magnitude of 10^{-7} or 10^{-8} solar masses per year. Additionally, other studies claim accretion rates around $\dot{M} \approx 10^{-6}$ - 10^{-7} $M_{\odot} yr^{-1}$ [27]. These values for the outflow and accretion rates are consistent with the literature. Particularly, it has been shown that both the mass outflow and accretion rates are related, and latter is usually an order of magnitude larger than the former [27]. Consequently, we used values within these ranges in our simulations.

2.2.2 Passive Disk and dust properties

The Disk Wind model that we are using has a large, flat and optically thick disk [2]. For our specific model, this disk extends from the sublimation radius R_{sub} (explained in 2.2.3) to $R_{out} = 43$ AU [10]. We assume that the grains of dust that make up the disk have all a spherical shape and a single size. Following previous applications of this model, we decided to use dust grains with a size of 1.0 μm, as these grains cool more effectively and can reach sublimation temperatures that correspond to a smaller sublimation radius [2]. This size is

also the demonstrated upper limit of dust size that winds of the types that we are considering is able to uplift [23], and thus, it serves as an upper limit of the possible SED that can be produced using the Disk Wind model. Notice that using a single size for the grains of dust is a simplification. However, we justify this decision as our desire is to focus more on the effects that the inclination and outflow rates have on the simulated SED, and it also allows us to make a more direct comparison to the HAe stars that were previously modeled with centrifugally driven winds [2].

2.2.3 Sublimation radius R_{sub}

A very important parameter in the model is the sublimation radius. As explained, passive disks posses a significant inner radial boundary within which no dust can reside. This is caused by the high temperatures in the vicinity of the central star, that are above the dust's sublimation temperature. A correct choice of the sublimation temperature is of great importance, as distinct sublimation radii may produce significantly different SED. Following the previous applications of the code we are using, we calculate the sublimation radius R_{sub} using the following equation [2]:

$$R_{sub} = H(T_*, T_{sub}, a)(L_*/L_\odot)^{1/2} T_{sub}^{-2} \quad AU \tag{2.1}$$

In equation 2.1, H is a scaling function dependent on the star's effective temperature T_*, the sublimation temperature T_{sub}, and the size of the grains of dust a. As we explained in subsection 2.2.2, we chose using grains of dust with a size of 1 μm. Thus, we justify using a $T_{sub} = 1850K$, consistent with the best geometric fits of passive disks obtained using a

$T_{sub} = 1800K$ [3]. Using previous calculations for the scaling function, we get a value of $H = 1.09e5$ [2]. Using a $L_* = 38900\ L_\odot$for MWC 297's [16], we obtain a sublimation radius $R_{sub} = 6.281$ AU.

2.2.4 Non-Stellar Emissions within R_{sub}

As stated in Chapter 1, some of the earliest studies suggested that MWC 297's NIR excess could be explained with accretion disks [8] [28] [29]. Even though the recent LBTI imaging of MWC 297 clearly demonstrates that an accretion disk by itself is insufficient to explain the observations, there is still a lot of value in modeling non-stellar emissions within the sublimation radius. To do so, we have explored two additional scenarios.

2.2.5 An inner accretion disk

Since the unmodified Disk Wind model that we are considering has an inner cavity, we have decided to separately calculate the contribution that an accretion disk inside R_{sub} would produce. Traditionally, the flux contribution from circumstellar disks with different morphologies has been modeled with Alpha-Disks (AD), where it is assumed that the disk is heated by stellar radiation and accretion [30]. To calculate the SED contribution from the accreting disk, the model separates it into several annuli, and it is assumed that each annuli radiates as a blackbody. The temperature for each annulus is then determined by the disk's temperature profile, which in the case of AD is given by $T(R) \propto R^\alpha$, where different values of α represent different disk morphologies. There are three free parameters in this model: α, r_{in} and r_{out}. Accretion disks are usually modeled with $\alpha = -0.75$, a value that corresponds

to a flat and optically thick disk [29] [31]. We explored using different values for r_{in}, but tried to keep it as small as possible to agree with the difficulty that some studies have had in resolving an inner gap [15], and we set r_{out} to be equal to the sublimation radius to prevent an overlap between the accretion disk and the passive disk that is already simulated with the MCRT code.

2.2.6 A smaller R_{sub}

With a more geometric fit in mind (rather than a physically motivated one) we also considered simply reducing the sublimation radius. Some studies have suggested that an opaque and inner gaseous disk could provide some shielding to the outer circumstellar structure. This shielding could effectively lessen the heating power of the star, allowing dust grains to be found within our calculated R_{sub} [29]. While just reducing the sublimation radius without adding another component to our Disk Wind model compromises its physical self-consistency, exploring how changing the sublimation radius affects the results may enrich the results of this and future studies.

Evidently, to effectively explore the different scenarios, a large number of models that cover a significant portion of the parameter space is required. Table 2.1 shows a summary of the major parameters in our models along with their respective values that we used in this study.

Param.	Units	Range
Wind Type	-	C, E, G
R_{sub}	AU	3.00 - 6.28
R_{out}	AU	43.0
z_{max}	AU	5.0
$\dot{M}$	$M_{\odot} yr^{-1}$	1×10^{-8} - 35×10^{-8}
a	μm	1.0
r_{in}	AU	$0.5 - 4.5$
r_{out}	AU	6.28

Table 2.1: A summary of the free parameters with their ranges of values that we explored in this study.

Chapter 3

Methodology

3.1 Monte Carlo Radiative Transfer

To create these models we use an already existing Monte Carlo Radiative Transfer (MCRT) code. MCRT is a method that uses random number generation and pre-selected probability distributions to simulate the creation, paths and events (absorption and scattering) that a large number of photon packets have in the modeled system. In our case, a large number of photon packets with different wavelengths are sampled according to the star's blackbody radiation. These photon packets leave the source at random angles, and then, they may enter a zone within the wind or disk. If this happens, the photon packets have three possibilities: undergoing a scattering event, undergoing an absorption event, or not undergoing any event. In the case of a scattering event, the photon is simply given a new random angle which assigns it a new path. In case an absorption, the photon packet is re-emitted with a new wavelength and it is assigned a new random angle. The probability that each of these events happens within a singular zone is a function of the grain opacities,

and the zone's density and temperature. Each zone's properties are not constant throughout the simulation, as absorption events change the temperature of a zone according to the conservation of energy. After a few iterations of this process, each photon packet eventually leaves the system. Binning these wave packets by their wavelength and angle provides a Spectral Energy Distribution that we can use to model MWC 297's SED. Since the analytic approximations that we are using to model the wind assume an axis-symmetric disk outflow [24], the code only simulates a 2D slice of the disk and wind (that still captures the photons' trajectories in 3D space). A more detailed explanation of the MCRT code that we use can we found in the original paper [2]. We did make a few modifications to this code. Namely, we generalized it to be useful for modeling higher luminosity stars and we added the ability to produce images at a variety of different inclinations (explained in 3.3).

3.2 Adding an inner disk to the Spectral Energy Distribution

As explained in Chapter 2, we also decided to use an Alpha-Disk to separately model an accretion disk within R_{sub} and add it to the output produced by the MCRT code. Following previous studies that have explained NIR interferometric measurements of HAeBE stars [14], the temperature profile of our accreting disk is given by:

$$T_{disk}(R) = T_{1AU} R^{-3/4} \tag{3.1}$$

Where R is the distance from the star to the annulus (in AU) and T_{1AU} is the temperature

of the disk at a distance of 1 AU from the source. Typically, T_{1AU} is typically determined by:

$$T_{1AU} = T_{sub} R_{sub}^{3/4} \tag{3.2}$$

Using the values calculated in Subsection 2.3.3, we get $T_{1AU} = 7340K$. Finally, to obtain the disk's SED, we add the blackbody radiation from each annuli weighted by their respective areas. That is, the disk's flux at a specific wavelength F_λ is given by:

$$F_\lambda = \sum_{i=1}^{n} A_i f_{\lambda,i} \tag{3.3}$$

Where A_i is the area of the ith annulus, $f_{\lambda,i}$ is the ith annulus' flux contribution at the wavelength λ (calculated with Planck's Function), and where the disk is separated into n annuli. Figure 3.1 shows the temperature profile used to model an accretion disk around MWC 297, as well as an illustrative example of how the contribution of an accreting disk can modify the observed SED for a star with similar properties to MWC 297.

3.3 Image Creation

As already stated, we made a slight modification to the MCRT code to obtain an additional output containing the position of each zone in the wind and disk, along with the number of wave packets with wavelengths in the 2.0-2.4 μm range that were emitted from them. This wavelengths correspond to the K-band, and we chose it because a considerable proportion of observational data (for MWC 297 and other similar objects) is likely to be at

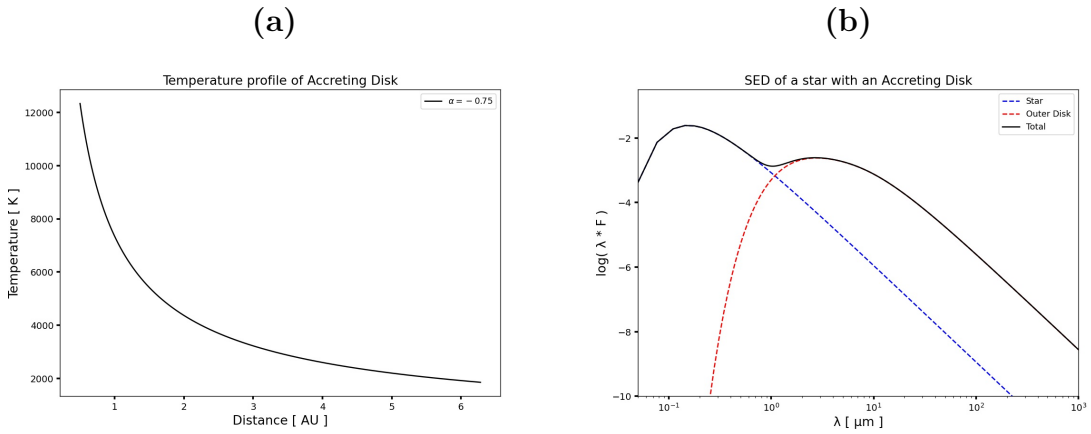

Figure 3.1: **(a)** shows the temperature profile used for the accreting disk around a star with similar properties to MWC 297. **(b)** is an example of the combined SED of a star and an accreting disk with $r_{in} = 1.0$ AU and $r_{out} = 50.0$ AU.

wavelengths close to the this band. As explained in Section 3.1, this provides us a 2D slice of the model that we can then use to create images at a specific wavelength. To do so, the first step is to create a 3D representation of our model using the simulated slice.

Suppose that we can represent each zone on a Cartesian 3D space with a vector $\vec{u} = \langle x, y, z \rangle$, where x, y and z are the zone's coordinates. Imagine then that the simulated 2D slice lays on the xz-plane (implying that $y = 0$ for all the simulated zones). Using cylindrical coordinates, extending the slice to create the three-dimensional model is given by:

$$x_{3D} = x_{2D} \cos\theta \tag{3.4}$$

$$y_{3D} = x_{2D} \sin\theta \tag{3.5}$$

$$z_{3D} = z_{2D} \tag{3.6}$$

The next step is to project the 3D coordinates onto a plane that has a normal $\vec{n}$ pointed towards the observer (thought to be located somewhere in the positive xz-plane). We know

that the parallel projection of vector $\vec{u}$ onto a plane with a normal $\vec{n}$ is equal to $\vec{n}\times(\vec{u}\times\vec{n})/|\vec{n}|^2$, which can also be written as:

$$\vec{u}_{||} = -\vec{n} \times (\vec{n} \times \vec{u})/|\vec{n}|^2 \tag{3.7}$$

Using the matrix representation of the cross product, an making $|\vec{n}| = 1$, we get

$$\vec{u}_{||} = \begin{bmatrix} n_z^2 + n_y^2 & -n_x n_y & -n_x n_z \\ -n_y n_x & n_z^2 + n_x^2 & -n_y n_z \\ -n_z n_x & -n_z n_y & n_x^2 + n_y^2 \end{bmatrix} \begin{bmatrix} u_1 \\ u_2 \\ u_3 \end{bmatrix} \tag{3.8}$$

Using $\vec{n} = \langle \sin i, 0, \cos i \rangle$, where i is the inclination at which the observer sees the disk-wind, we finally get the following expression:

$$\vec{u}_{||} = \begin{bmatrix} \cos^2 i & 0 & -\sin i \cos i \\ 0 & 1 & 0 \\ -\cos i \sin i & 0 & \sin^2 i \end{bmatrix} \begin{bmatrix} u_1 \\ u_2 \\ u_3 \end{bmatrix} \tag{3.9}$$

The only step to create an image that is left is to bin the projected zones. We decided to bin the projected points in both square and polar bins. Figures 3.2 and 3.3 show the images created of a simulated outflow around AB Aur, a Herbig Ae star that has been previously modeled with the same MCRT code we use in this study [2]. For simplicity, we have not extended the model to include the bottom half.

(a)

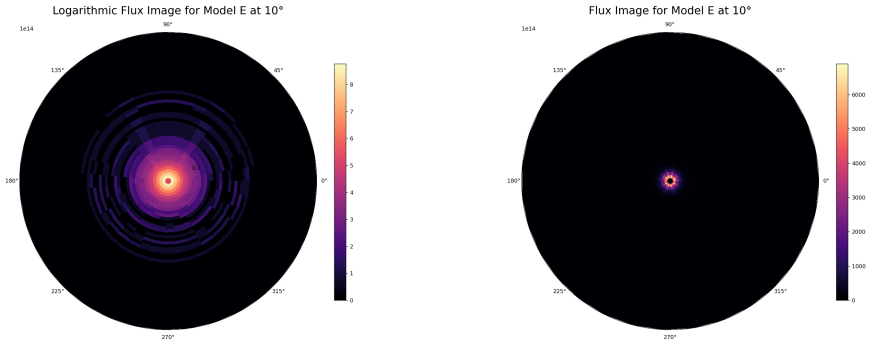

(b)

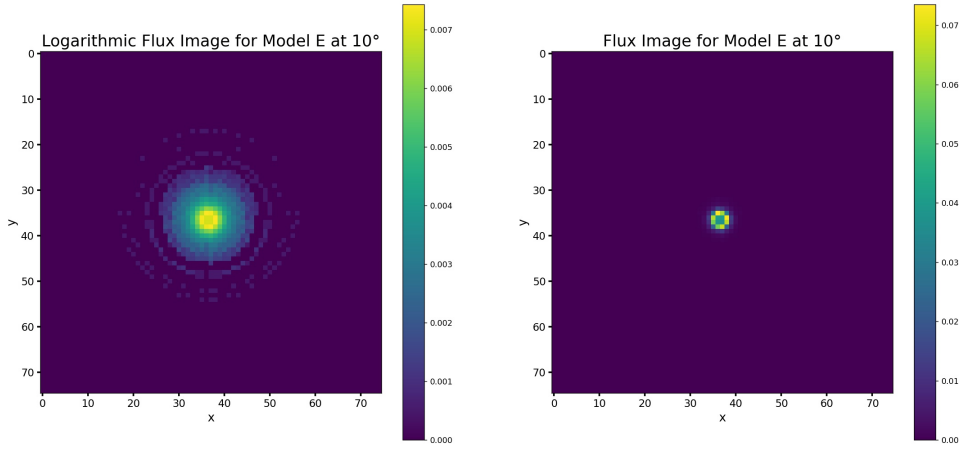

Figure 3.2: Created images of a simulated outflow around AB Aur, a Herbig Ae star that has been correctly modeled with this MCRT code [2] observed at an inclination $i = 10°$. **(a)** shows the images created with polar bins, while **(b)** shows the same images created using Cartesian bins. These images do not show the main source at the center, nor the bottom half of the expected bipolar outflow.

(a)

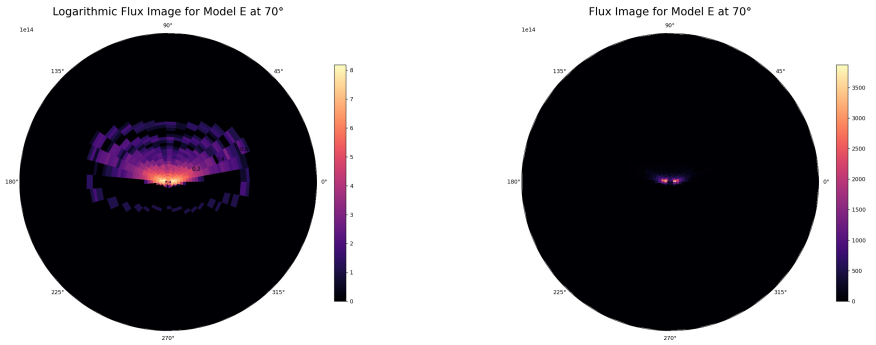

(b)

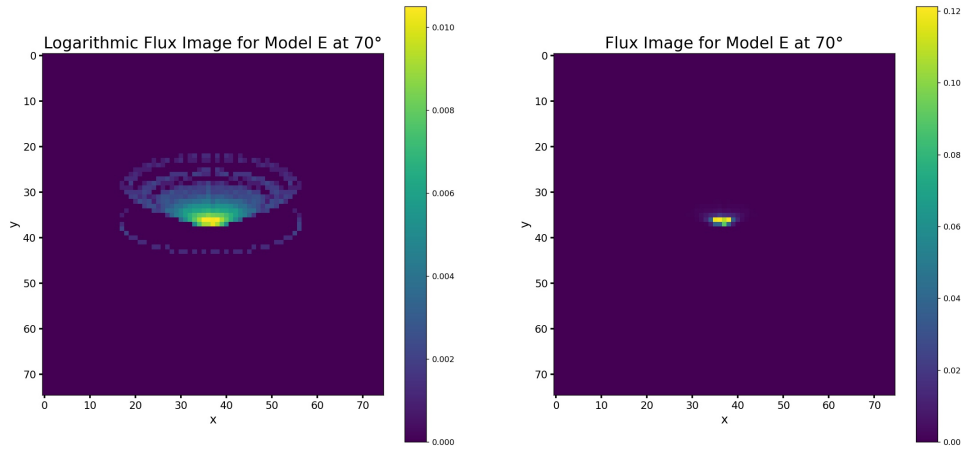

Figure 3.3: Created images of a simulated outflow around AB Aur, a Herbig Ae star that has been correctly modeled with this MCRT code [2] observed at an inclination $i = 70°$. **(a)** shows the images created with polar bins, while **(b)** shows the same images created using Cartesian bins. At this inclination, it is noticeable that the outflow lays above the disk's plane. These images do not show the main source at the center, nor the bottom half of the expected bipolar outflow.

Chapter 4

Results and Discussion

4.1 Spectral Energy Distributions

The following results represent a sample of the SED obtained from the different models in this study. For comparison, plotted with all of our simulated SED is the observational data taken by the Very Large Telescope Interferometer [29]. The first major result that we obtained was an upper limit on the inclination that our models were at least somewhat satisfactorily fitting MWC 297's SED. Figure 4.1 shows a single simulation of a Wind-Disk seen at different angles. As we can appreciate, major under-fluxes in the NIR are observed at angles $\geq 50°$, something that we observed in all of the simulations that we performed. We believe that these under-fluxes are caused by the wind itself. At higher inclinations, the wind covers a larger area in the observer's line of sight. Consequently, any photons originally traveling towards the observer have a high probability of interacting with the wind, which ultimately causes them to escape the simulated system at angles corresponding to lower inclinations. Moreover, these photons could be absorbed by the cooler back end of the wind,

causing them to be re-emitted at wavelengths that are longer than what we are tracking. Indeed, using the values reported in Table 2.1, $\tan^{-1}(z_{max}/R_{sub}) \approx 40°$, which supports the idea that at inclinations $\geq 50°$, the wind is on the line of sight between the observer and the main source. Unfortunately, this means that many of the best models where the wind alone can reproduce the NIR flux without the need for implausibly high outflow rates also imply very high rotational speeds for MWC 297 (the $v\ sin\ i$ inconsistency, see Chapter 1). Certainly, increasing the values for some of the other model parameters (such as outflow rate, sublimation radius and the contribution of an inner disk) could allow us to get the NIR fluxes present in the observational data. However, simply changing these parameters without good justifications may lead to unphysical values. Thus, to alleviate this as much as possible, all the following results mainly consider outputs where the inclination is $i = 40°$. In consequence, the values we obtain for other model parameters (specially the outflow rate) may represent lower limits.

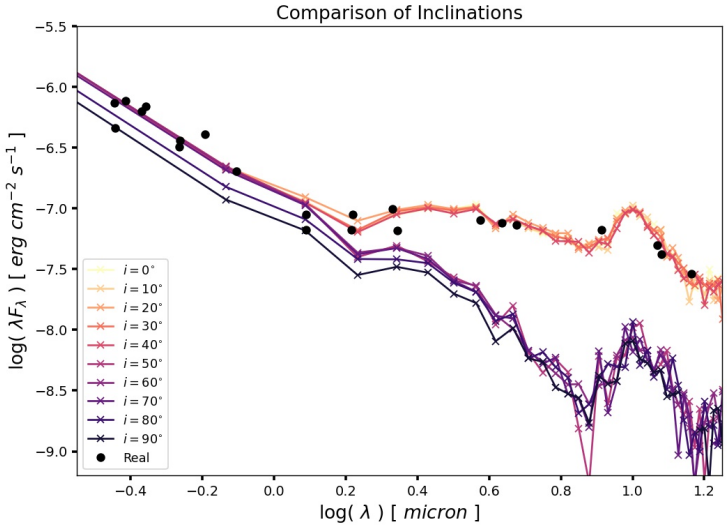

Figure 4.1: A comparison of the same model seen at different inclinations. Evidently, inclinations $\geq 50°$ have severe under-fluxes, which imposes an upper limit for the inclinations in our models. The parameters used in this model can be seen in Table 4.1 (WD).

Figures 4.2 to 4.4 show the SED for a variety of outflow rates using the unmodified Disk-Wind models. As we would expect, a lower outflow rate produces a lower NIR excess. We can also appreciate that when $\dot{M} \approx 30 \times 10^{-8}\ M_{\odot} yr^{-1}$, the simulated SED start becoming comparable to MWC 297's observational data in all three cases. Comparing across these figures makes it evident that Model C requires lower outflow rates to have a NIR excess similar to the observational data, which is what we expected (see Section 2.2). Notice that wind type G produces the lowest NIR, also as expected. Compared to the previous applications of this MCRT code to model HAe stars with considerably less luminosity than MWC 297, we see that much higher outflow rates are needed with a higher luminosity star (about an order of magnitude of difference) [2]. This can be explained by the larger sublimation radius around MWC 297. Larger values of R_{sub} imply that the dusty wind launches at a larger distance from the source, and consequently, the wind's density is significantly lower, as it declines with larger a larger radial distance [2]. Additionally, MWC 297's higher mass leads to a naturally higher difficulty to leave the disk given the higher gravitational field, as the density profiles that we have used decline with increased mass [2]. Despite this, HBe sources are generally associated with higher accretion and outflow rates, making these results completely consistent [32].

Moving to the models with non-stellar emissions within R_{sub}, Figure 4.5 shows a small sample of the SED we obtained by adding a variety of different disks inside the sublimation radius to distinct simulated outflows. It is evident that the inner radius of the externally calculated disk r_{in} greatly influences the disk's radiation, as smaller values of r_{in} shift the disk's SED towards shorter wavelengths. Comparing these SED to those of the unmodified Disk-Wind models, we clearly appreciate that the inner disk produces the most relevant changes

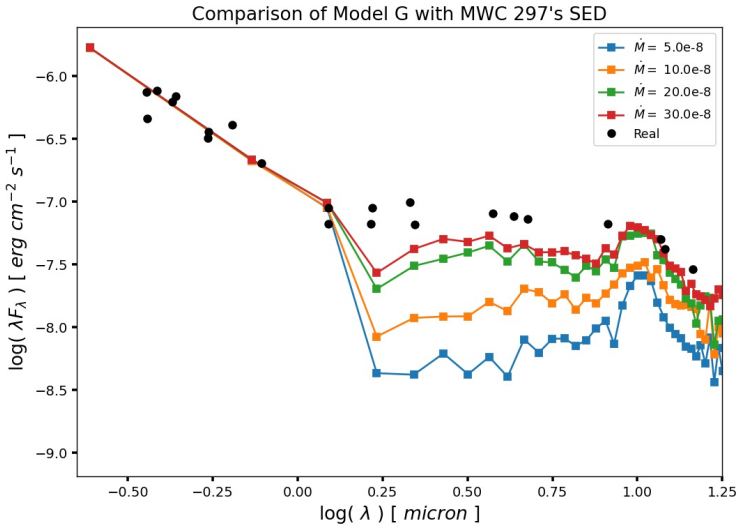

Figure 4.2: A comparison Model G with different outflow rates, all observed at an inclination $i = 40°$.

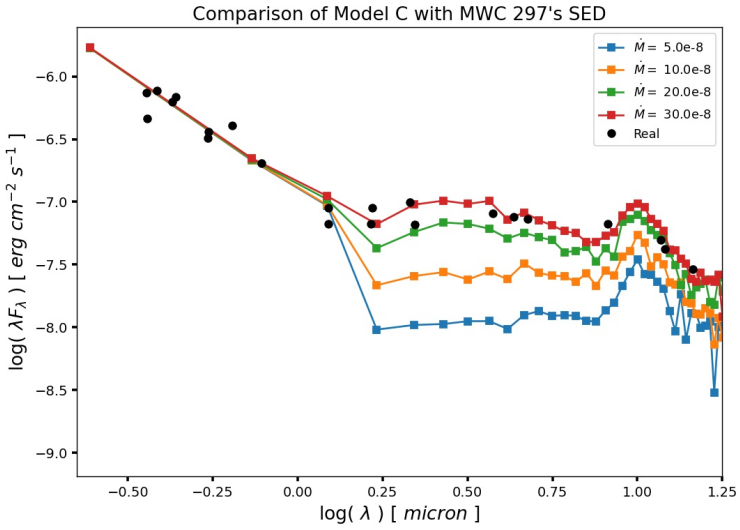

Figure 4.3: A comparison Model C with different outflow rates, all observed at an inclination $i = 40°$.

at $log(\lambda)$ values around 0.25. However, the outflows still remain the major contributor to the excess at longer wavelengths, which demonstrates that the outflows are undoubtedly relevant even in the presence of an inner accretion disk.

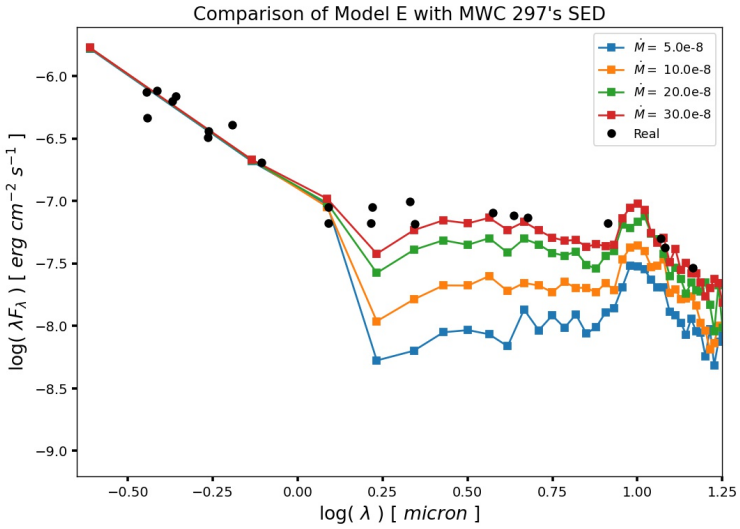

Figure 4.4: A comparison Model E with different outflow rates, all observed at an inclination $i = 40°$.

Lastly, Figure 4.5 also shows two examples of SED obtained by using smaller sublimation radii for the Disk-Wind model. As expected, even moderate outflow rates are able to produce a NIR excess comparable to the observational data.

4.2 Best Models

Exploring different models with several free parameters certainly led to a degeneracy of results. For instance, the SED produced by Model E with higher outflow rates can lead to similar results produced by model C with lower outflow rates, and the addition of an accretion disk typically decreased the outflow rate required with any wind type by a factor of two to correctly match the observational data. However, we decided to choose the best models from each scenario to keep the discussion focused. Qualitatively, we have defined that a model is a good fit if it matches the main characteristics of the observational data.

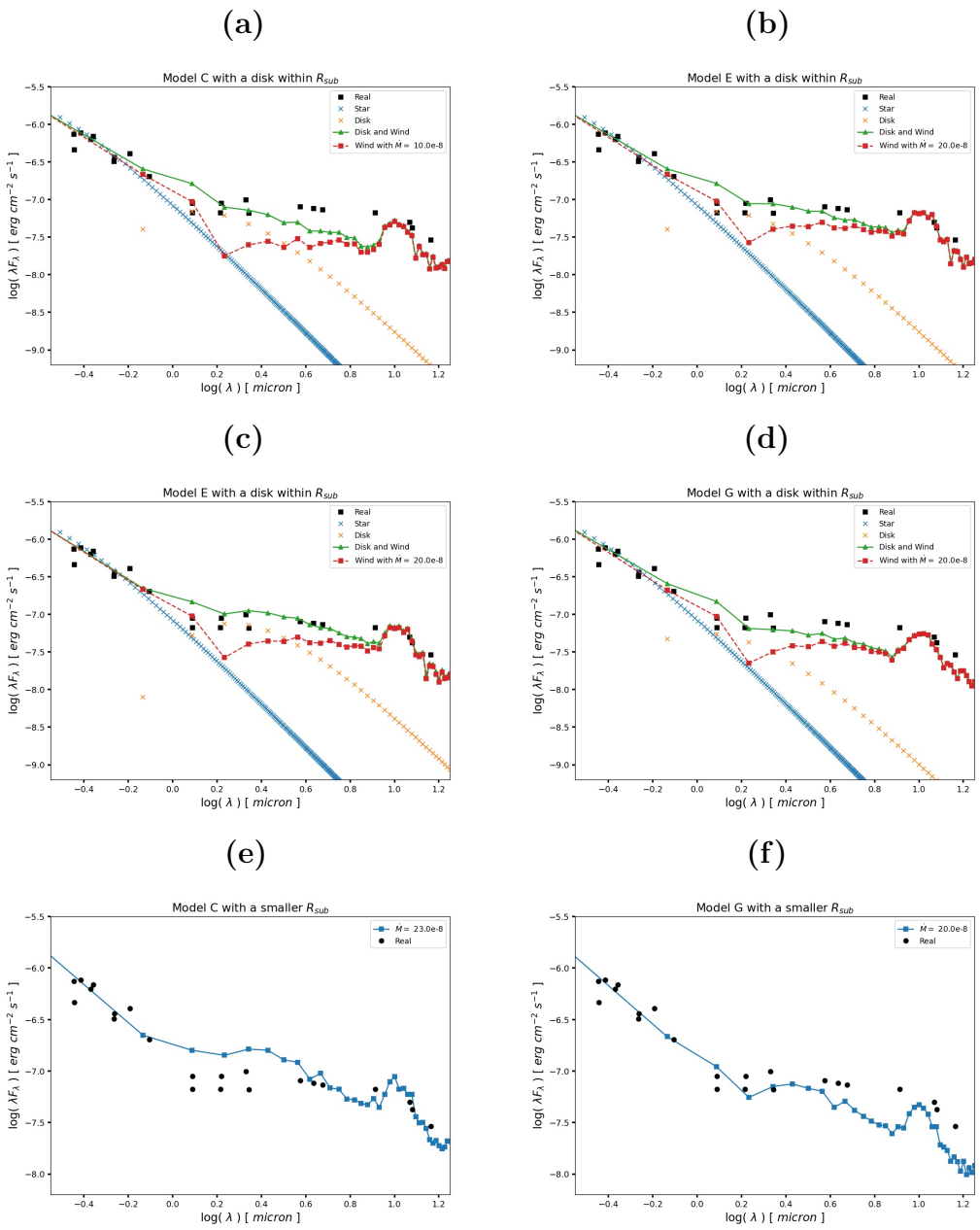

Figure 4.5: Distinct examples of models with non-stellar emissions within the sublimation radius, all observed at an inclination $i = 40°$. **(a)** shows Model C with an $\dot{M} = 10 \times 10^{-8}$ $M_{\odot}yr^{-1}$ and $r_{in} = 2.0$ AU. **(b)** shows Model E with an $\dot{M} = 20 \times 10^{-8}$ $M_{\odot}yr^{-1}$ and $r_{in} = 2.2$ AU. **(c)** shows Model E with an $\dot{M} = 10 \times 10^{-8}$ $M_{\odot}yr^{-1}$ and $r_{in} = 5.2$ AU. **(d)** shows Model G with an $\dot{M} = 10 \times 10^{-8}$ $M_{\odot}yr^{-1}$ and $r_{in} = 1.5$ AU. **(e)** shows Model C with an $\dot{M} = 23 \times 10^{-8}$ $M_{\odot}yr^{-1}$ and $R_{sub} = 2.5$ AU. **(f)** shows Model G with an $\dot{M} = 20 \times 10^{-8}$ $M_{\odot}yr^{-1}$ and $R_{sub} = 3.5$ AU. Notice how the wind type, R_{sub}, r_{in}, and $\dot{M}$ are all very influential parameters for the final SED.

Name	Wind Type	R_{sub} [AU]	$\dot{M}$ $[M_\odot yr^{-1}]$	r_{in} [AU]
`WD`	C	6.281	$30^{+5}_{-5} \times 10^{-8}$	-
`WD+Acc`	C,E	6.281	$25^{+5}_{-5} \times 10^{-8}$	0.5
`WD-R`	E	3.140	$23^{+5}_{-5} \times 10^{-8}$	-

Table 4.1: Models with the best qualitative fits from this study. The names are representative: `WD` is the unmodified Wind-Disk model, `WD+Acc` is the Wind-Disk model with an inner accretion disk, and `WD-R` is the Wind-Disk model with a smaller sublimation radius.

Furthermore, the correctness of a model is also weighted by how physically justifiable are the parameters used to create it. With these criteria, Table 4.1 shows the parameters of the best models from our study (the first column contains the names that we have assigned to these models for an easier discussion), and Figure 4.6 shows the Spectral Energy Distributions for these three models.

4.2.1 Model `WD`

The attractiveness of this model lays on its simplicity compared to `WD+Acc` and `WD-R`, as its creation did not require any major modifications to the MCRT code. This makes this model almost entirely self-consistent. However, the major drawback is the wind type. MWC 297 is significantly more luminous than the stars that were previously modeled with the MCRT code that we are using [2]. Consequently, the code neglects any effects that the radiative pressure may produce in the wind's morphology. It is possible that this effect is not negligible in the case of stars as luminous as MWC 297, and thus, we would expect the wind lines to be further bent outwards. The only representative way in which we can consider this effect is by changing the wind type from model C to model E, as this could approximately show what the radiative pressure may do to the wind lines. A disadvantage arises at this point, however. Even with model C, `WD` requires a high outflow rate ($\dot{M} = 30 \times 10^{-8}\ M_\odot yr^{-1}$)

(a)

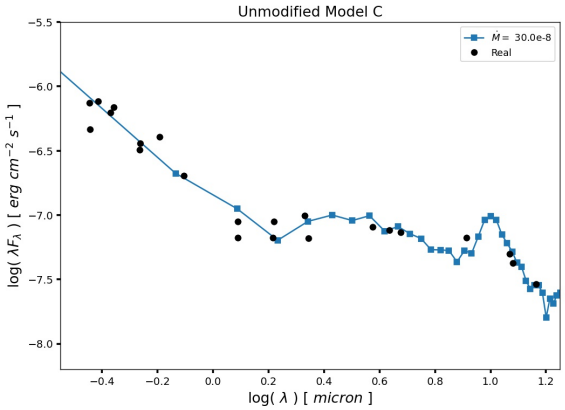

(b)

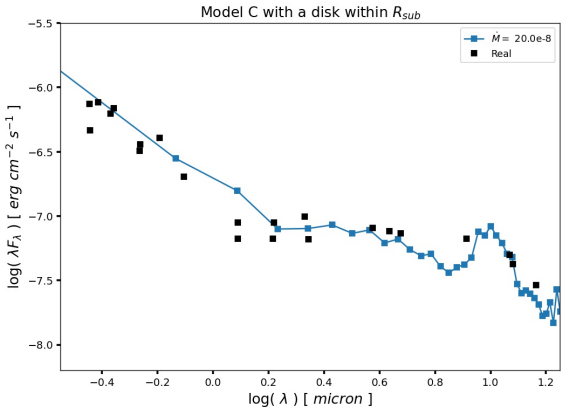

(c)

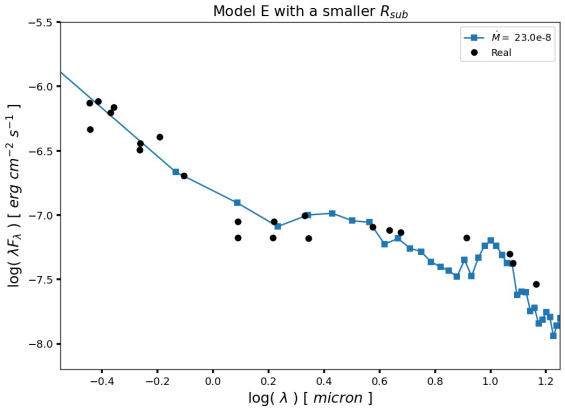

Figure 4.6: Spectral Energy Distributions for the best three models. **(a)** Model `WD` with $\dot{M} = 30 \times 10^{-}8\ M_{\odot} yr^{-1}$. **(b)** Model `WD+Acc` with wind type C and $\dot{M} = 20 \times 10^{-}8\ M_{\odot} yr^{-1}$. **(c)** Model `WD-R` with $\dot{M} = 23 \times 10^{-}8\ M_{\odot} yr^{-1}$.

that is already close to the measured upper limit [27]. Changing the wind type to Model E would only worsen the situation, as model E requires higher outflow rates to match the NIR that Model C produces. These reasons may suggest that a radiatively bent wind on its own might require outflow rates that are higher than what the literature suggests to explain the observational data. Figure 4.7 shows the recreated images for this model. We did not use the images to evaluate the quality of these models, as our only comparison is a reconstructed image (Figure 1.1). Notice, however, that all the images that we show for our models present the expected asymmetries seen in moderately inclined outflows.

4.2.2 Model `WD+Acc`

Being the most complex model that we are considering, Model `WD+Acc` tries to bring old and new observations of MWC 297's NIR excess together. As we can appreciate in Figure 4.8, the inner disk helps create a better fit for an unmodified Wind-Disk model of type C, but at the expense of producing an over-flux at $log(\lambda) \approx 0.1$ (a feature not seen in the observational data). Another advantage to this mode is that it possesses the lowest outflow rate ($20 \times 10^{-8}\ M_{\odot} yr^{-1}$) out of the best models. Notice that, similar to model `WD`, using the other wind types could reproduce similar results by using outflow rates that might be above the upper limit for MWC 297 [27], or require a disproportionate contribution for the inner disk. Returning to Model C, the major drawback of this model is its lack of self-consistency. Externally calculating a disk within the sublimation radius and adding it to the output of the MCRT code compromises the physical validity of the model. For instance, an optically thick disk within the sublimation radius might provide some shielding that allows the dusty

(a)

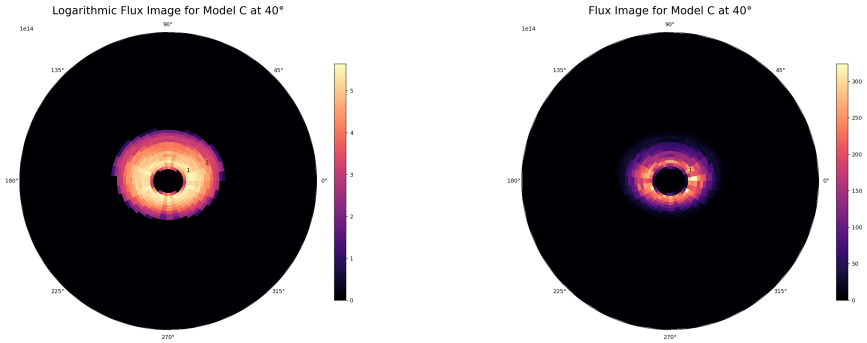

(b)

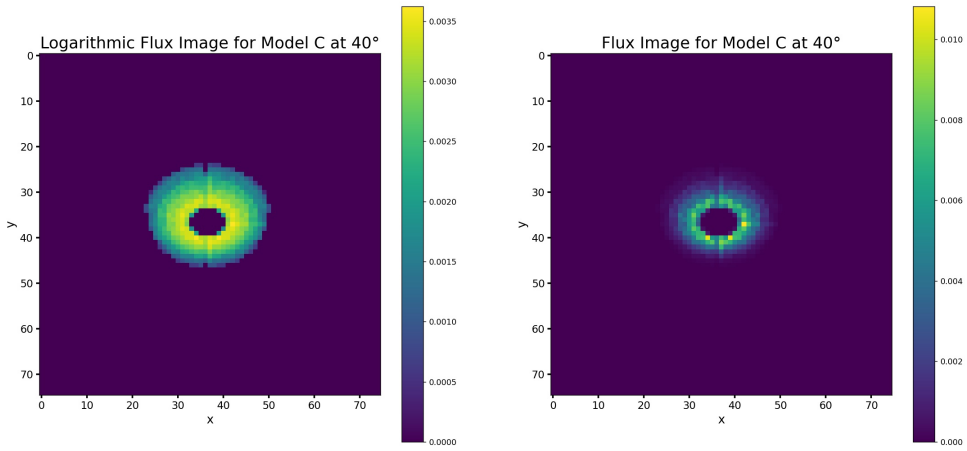

Figure 4.7: Created images of Model `WD`. **(a)** shows the images created with polar bins, while **(b)** shows the same images created using Cartesian bins.

wind to exist at a closer distance from MWC 297 [29][28], an effect that we are not taking into account here. Additionally, the accretion disk's emission provides a secondary source of photons that the wind and passive disk could intercept. However, the accretion disks that we have used have a flux that is primarily composed of photons with wavelengths of $\approx 1.0\mu m$, and the oppacities of the grains that make up the passive disk and wind decreases at these longer wavelengths [2]. Consequently, we justify that our implementation is a good approximation. Taking the proportion of fluxes coming from the disk and star, we get a value of $F_{disk}/F_{star} \approx 0.068$, which is well within the observed values in other HAeBe stars [33].

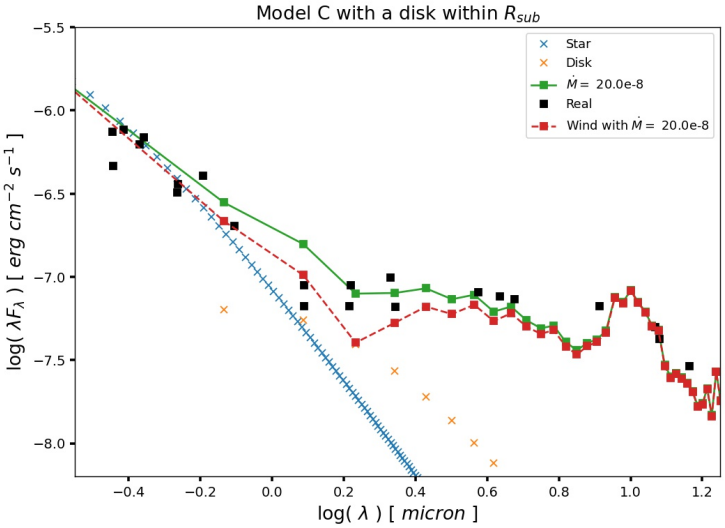

Figure 4.8: Detailed SED components for Model `WD+Acc`.

4.2.3 Model `WD-R`

This model presents an interesting scenario, although it is possibly the least physically motivated. Model `WD-R` makes a satisfactory fit for almost the entirety of the observational

data. It does show a small over-flux at $log(\lambda) \approx 0.1$, but it is less noticeable than in the case of Model `WD+Acc`. Two other major advantages of this model are the wind type (most outwardly bent of the three types, which makes it qualitatively more consistent with higher luminosity sources) and the moderate outflow rate. However, the self-consistency of this model is also compromised. Here again, the presence of an optically thick structure within the sublimation radius may allow the dusty wind to launch closer to the source [28] [27]. Thus, combining models `WD+Acc` and `WD-R` in a physically consistent manner may yield better results. Figure 4.9 shows the recreated images for this model.

4.3 Discussion

MWC 297 remains a challenging object to model. We can conclude that magnetically supported outflows alone require high outflow rates to satisfactorily explain MWC 297's NIR excess and interferometric images. Despite this disadvantage, these outflows did demonstrate playing an important role at producing the observational data at longer wavelengths. Furthermore, considering models with non-stellar emissions within the sublimation radius proved to be fruitful. Models like this bring together both the old and new interpretations of MWC 297's NIR excess. However, if dusty winds (with or without non-stellar emissions within R_{sub}) are responsible for the NIR excess, then moderately edge on inclinations remain hard to justify, as higher inclinations require mass outflow rates that may be in conflict with previously reported values.

Moreover, this study does show that exploring models with higher complexities may improve the explanations for the observational data and a lot of new possibilities are still left

(a)

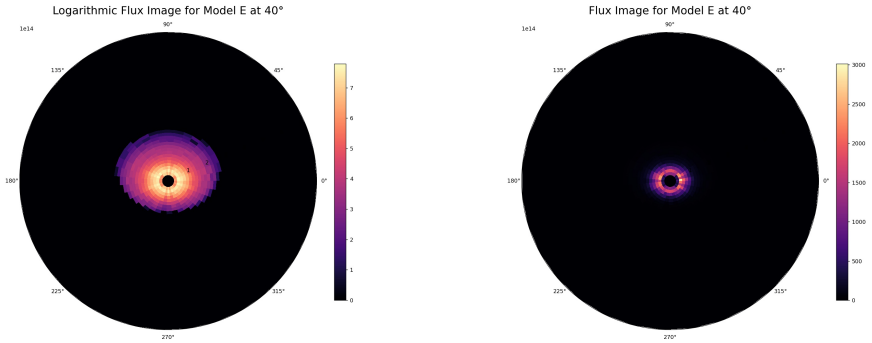

(b)

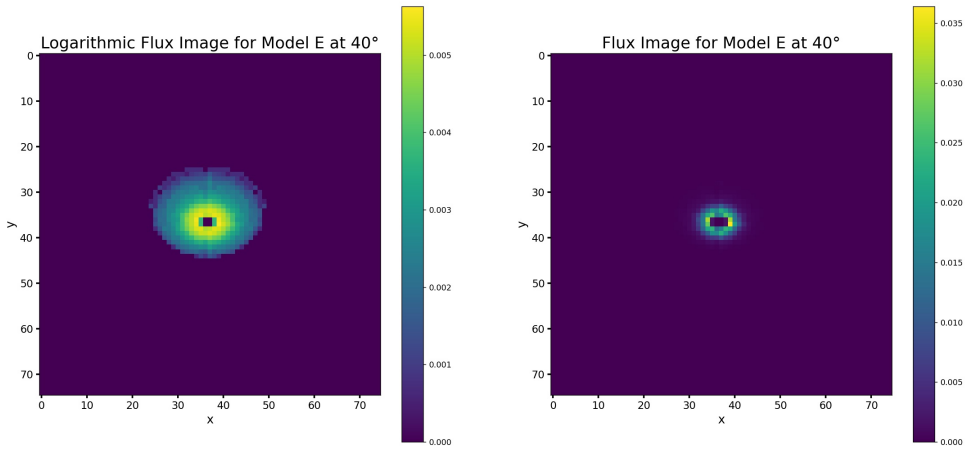

Figure 4.9: Created images of Model `WD-R`. **(a)** shows the images created with polar bins, while **(b)** shows the same images created using Cartesian bins.

open to be explored. Expanding the modelling of the circumstellar environment around higher luminosity stars with similar approaches may improve our understanding of the underlying physical mechanisms that govern the late stages of star formation, as well as the environment in which active planet formation may be taking place.

4.3.1 Future Work

As explained, there are certainly many new venues to explore that stem from this study. Four major directions that could extend the results presented in this work are:

- Consider other high luminosity stars: Modeling other known Herbig Be stars with the models that we have presented would help us to generalize our results. Moreover, improving the image reconstruction would allow us to make better comparisons with interferometric images from other high luminosity sources, and it would allow us to probe its value as a diagnostic tool.

- Treatment of the radiation pressure and its effects on the Wind morphology: Creating new density profiles for these Disk-Wind models that take into account the effect that the radiative pressure may have on the wind's morphology would allow for a more physically consistent model. It would also allow us to understand how influential radiation pressure is in the case of higher luminosity stars. Related to this, exploring models with thicker winds is also worthwhile, as the models that we have used consider thin winds justified by the lack of ionizing flux that is able to travel through the wind's dusty layers (something that worked with lower luminosity stars [2]). However, MWC 297's luminosity may still be able to ionize particles that are considerably farther out

than what we have considered in this study.

- A self-consistent implementation of an accretion disk: Instead of adding an externally calculated disk within the sublimation radius, a direct implementation of an accretion disk to the existing MCRT code may improve the physical consistency of this scenario. This would also allow us to explore the effects that an inner gaseous outflow coming from this disk may have in the final SED, something that has been explored with lower luminosity stars [2].

- Examining longer wavelengths: Studying the effects that these models may have at longer SED wavelengths (millimeter range) might require an extension of the physical extent that that the simulations take into account. This would be more computationally expensive, but it would also allow us to investigate the circumstellar structure around HAeBe stars associated with these wavelengths.

Bibliography

[1] S. Sallum, J. A. Eisner, J. M. Stone, J. Dietrich, P. Hinz, and E. Spalding, "ELT Imaging of MWC 297 from the 23 m LBTI: Complex Disk Structure and a Companion Candidate," , vol. 161, p. 28, Jan. 2021.

[2] A. Bans and A. Königl, "A Disk-wind Model for the Near-infrared Excess Emission in Protostars," , vol. 758, p. 100, Oct. 2012.

[3] T. Alonso-Albi, A. Fuente, R. Bachiller, R. Neri, P. Planesas, L. Testi, O. Berné, and C. Joblin, "Circumstellar disks around Herbig Be stars," , vol. 497, pp. 117–136, Apr. 2009.

[4] A. Sargent and S. Beckwith, "Disks Around T Tauri Stars," vol. 59, p. 203, Jan. 1994.

[5] G. H. Herbig, "The Spectra of Be- and Ae-Type Stars Associated with Nebulosity," , vol. 4, p. 337, Mar. 1960.

[6] L. B. F. M. Waters and C. Waelkens, "Herbig ae/be stars," *Annual Review of Astronomy and Astrophysics*, vol. 36, no. 1, pp. 233–266, 1998.

[7] V. Piétu, A. Dutrey, and C. Kahane, "A Keplerian disk around the Herbig Ae star HD 34282," , vol. 398, pp. 565–569, Feb. 2003.

[8] F. Malbet, M. Benisty, W. J. de Wit, S. Kraus, A. Meilland, F. Millour, E. Tatulli, J. P. Berger, O. Chesneau, K. H. Hofmann, A. Isella, A. Natta, R. G. Petrov, T. Preibisch, P. Stee, L. Testi, G. Weigelt, P. Antonelli, U. Beckmann, Y. Bresson, A. Chelli, M. Dugué, G. Duvert, S. Gennari, L. Glück, P. Kern, S. Lagarde, E. Le Coarer, F. Lisi, K. Perraut, P. Puget, F. Rantakyrö, S. Robbe-Dubois, A. Roussel, G. Zins, M. Accardo, B. Acke, K. Agabi, E. Altariba, B. Arezki, E. Aristidi, C. Baffa, J. Behrend, T. Blöcker, S. Bonhomme, S. Busoni, F. Cassaing, J. M. Clausse, J. Colin, C. Connot, A. Delboulbé, A. Domiciano de Souza, T. Driebe, P. Feautrier, D. Ferruzzi, T. Forveille, E. Fossat, R. Foy, D. Fraix-Burnet, A. Gallardo, E. Giani, C. Gil, A. Glentzlin, M. Heiden, M. Heininger, O. Hernandez Utrera, D. Kamm, M. Kiekebusch, D. Le Contel, J. M. Le Contel, T. Lesourd, B. Lopez, M. Lopez, Y. Magnard, A. Marconi, G. Mars, G. Martinot-Lagarde, P. Mathias, P. Mège, J. L. Monin, D. Mouillet, D. Mourard, E. Nussbaum, K. Ohnaka, J. Pacheco, C. Perrier, Y. Rabbia, S. Rebattu, F. Reynaud, A. Richichi, A. Robini, M. Sacchettini, D. Schertl, M. Schöller, W. Solscheid, A. Spang, P. Stefanini, M. Tallon, I. Tallon-Bosc, D. Tasso, F. Vakili, O. von der Lühe, J. C. Valtier, M. Vannier, and N. Ventura, "Disk and wind interaction in the young stellar object ¡ASTROBJ¿MWC 297¡/ASTROBJ¿ spatially resolved with AMBER/VLTI," , vol. 464, pp. 43–53, Mar. 2007.

[9] J. C. Mottram, J. S. Vink, R. D. Oudmaijer, and M. Patel, "On the difference between Herbig Ae and Herbig Be stars," *Monthly Notices of the Royal Astronomical Society*, vol. 377, pp. 1363–1374, 04 2007.

[10] J. Drew, G. Busfield, M. Hoare, K. Murdoch, C. Nixon, and R. Oudmaijer, "Mwc 297,

bl.5ve: A zero-age main-sequence star in the aquila rift," *Monthly Notices of the Royal Astronomical Society*, vol. 286, pp. 538–548, 03 1997.

[11] P. J. McGregor, S. E. Persson, and J. G. Cohen, "Spectrophotometry of compact embedded infrared sources in the 0.6-1.0micron wavelength region.," , vol. 286, pp. 609–629, Nov. 1984.

[12] L. A. Hillenbrand, S. E. Strom, F. J. Vrba, and J. Keene, "Herbig Ae/Be Stars: Intermediate-Mass Stars Surrounded by Massive Circumstellar Accretion Disks," , vol. 397, p. 613, Oct. 1992.

[13] R. Millan-Gabet, F. P. Schloerb, and W. A. Traub, "Spatially Resolved Circumstellar Structure of Herbig AE/BE Stars in the Near-Infrared," , vol. 546, pp. 358–381, Jan. 2001.

[14] J. A. Eisner, B. F. Lane, R. L. Akeson, L. A. Hillenbrand, and A. I. Sargent, "Near-Infrared Interferometric Measurements of Herbig Ae/Be Stars," , vol. 588, pp. 360–372, May 2003.

[15] J. D. Monnier, J. P. Berger, R. Millan-Gabet, W. A. Traub, F. P. Schloerb, E. Pedretti, M. Benisty, N. P. Carleton, P. Haguenauer, P. Kern, P. Labeye, M. G. Lacasse, F. Malbet, K. Perraut, M. Pearlman, and M. Zhao, "Few Skewed Disks Found in First Closure-Phase Survey of Herbig Ae/Be Stars," , vol. 647, pp. 444–463, Aug. 2006.

[16] M. Vioque, R. D. Oudmaijer, D. Baines, I. Mendigutía, and R. Pérez-Martínez, "Gaia DR2 study of Herbig Ae/Be stars," , vol. 620, p. A128, Dec. 2018.

[17] M. G. Ubeira-Gabellini, V. Christiaens, G. Lodato, M. v. d. Ancker, D. Fedele, C. F. Manara, and D. J. Price, "Discovery of a Low-mass Companion Embedded in the Disk of the Young Massive Star MWC 297 with VLT/SPHERE," , vol. 890, p. L8, Feb. 2020.

[18] C. J. Burrows, K. R. Stapelfeldt, A. M. Watson, J. E. Krist, G. E. Ballester, J. T. Clarke, D. Crisp, I. Gallagher, John S., R. E. Griffiths, J. J. Hester, J. G. Hoessel, J. A. Holtzman, J. R. Mould, P. A. Scowen, J. T. Trauger, and J. A. Westphal, "Hubble Space Telescope Observations of the Disk and Jet of HH 30," , vol. 473, p. 437, Dec. 1996.

[19] S. Wolf, A. Schegerer, H. Beuther, D. L. Padgett, and K. R. Stapelfeldt, "Submillimeter Structure of the Disk of the Butterfly Star," , vol. 674, p. L101, Feb. 2008.

[20] A. S. Cotera, B. A. Whitney, E. Young, M. J. Wolff, K. Wood, M. Povich, G. Schneider, M. Rieke, and R. Thompson, "High-Resolution Near-Infrared Images and Models of the Circumstellar Disk in HH 30," , vol. 556, pp. 958–969, Aug. 2001.

[21] D. P. Stark, B. A. Whitney, K. Stassun, and K. Wood, "Near-Infrared Synthetic Images of Protostellar Disks and Envelopes," , vol. 649, pp. 900–913, Oct. 2006.

[22] R. E. Pudritz and C. A. Norman, "Centrifugally driven winds from contracting molecular disks," , vol. 274, pp. 677–697, Nov. 1983.

[23] P. N. Safier, "Centrifugally Driven Winds from Protostellar Disks. I. Wind Model and Thermal Structure," , vol. 408, p. 115, May 1993.

[24] R. D. Blandford and D. G. Payne, "Hydromagnetic flows from accretion disks and the production of radio jets.," , vol. 199, pp. 883–903, June 1982.

[25] P. N. Safier, "Centrifugally Driven Winds from Protostellar Disks. II. Forbidden-Line Emission in T Tauri Stars," , vol. 408, p. 148, May 1993.

[26] A. Konigl and J. F. Kartje, "Disk-driven Hydromagnetic Winds as a Key Ingredient of Active Galactic Nuclei Unification Schemes," , vol. 434, p. 446, Oct. 1994.

[27] G. Weigelt, V. P. Grinin, J. H. Groh, K. H. Hofmann, S. Kraus, A. S. Miroshnichenko, D. Schertl, L. V. Tambovtseva, M. Benisty, T. Driebe, S. Lagarde, F. Malbet, A. Meilland, R. Petrov, and E. Tatulli, "VLTI/AMBER spectro-interferometry of the Herbig Be star MWC 297 with spectral resolution 12 000," , vol. 527, p. A103, Mar. 2011.

[28] P. Manoj, P. T. P. Ho, N. Ohashi, Q. Zhang, T. Hasegawa, H.-R. Chen, H. C. Bhatt, and N. M. Ashok, "An Evolved Disk Surrounding the Massive Main-Sequence Star MWC 297?," , vol. 667, pp. L187–L190, Oct. 2007.

[29] B. Acke, T. Verhoelst, M. E. van den Ancker, P. Deroo, C. Waelkens, O. Chesneau, E. Tatulli, M. Benisty, E. Puga, L. B. F. M. Waters, A. Verhoeff, and A. de Koter, "MWC 297: a young high-mass star rotating at critical velocity," , vol. 485, pp. 209–221, July 2008.

[30] D. Lynden-Bell and J. E. Pringle, "The evolution of viscous discs and the origin of the nebular variables.," , vol. 168, pp. 603–637, Sept. 1974.

[31] C. P. Dullemond, "The 2-D structure of dusty disks around Herbig Ae/Be stars. I. Models with grey opacities," , vol. 395, pp. 853–862, Dec. 2002.

[32] C. Wichittanakom, R. D. Oudmaijer, J. R. Fairlamb, I. Mendigutía, M. Vioque, and

K. M. Ababakr, "The accretion rates and mechanisms of herbig ae/be stars," *Monthly Notices of the Royal Astronomical Society*, vol. 493, p. 234–249, Jan 2020.

[33] C. A. Grady, "The Circumstellar Disks of Herbig Ae/Be Stars," in *The Nature and Evolution of Disks Around Hot Stars* (R. Ignace and K. G. Gayley, eds.), vol. 337 of *Astronomical Society of the Pacific Conference Series*, p. 155, Nov. 2005.